

Grafting from versus *grafting to* approaches
for the functionalisation of graphene
nanoplatelets with poly(methyl methacrylate)

Noelia Rubio,[‡] Heather Au,[‡] Hannah S. Leese, Sheng Hu, Adam J. Clancy and Milo S.
P. Shaffer*

Department of Chemistry, Imperial College London, London SW7 2AZ, UK.

*Keywords: graphene, functionalisation, polymer, grafting from, grafting to,
poly(methyl methacrylate)*

Accepted: 19th August 2017

1 [*m.shaffer@imperial.ac.uk](mailto:m.shaffer@imperial.ac.uk)

2 ‡ Equal contribution

3 ABSTRACT Graphene nanoplatelets (GNP) were exfoliated using a non-destructive chemical
4 reduction method and subsequently decorated with polymers using two different approaches:
5 *grafting from* and *grafting to*. Poly(methyl methacrylate) (PMMA) with varying molecular
6 weights was covalently attached to the GNP layers using both methods. The grafting ratios were
7 higher (44.6% to 126.5%) for the *grafting from* approach compared to the *grafting to* approach
8 (12.6% to 20.3%). The products were characterised using Thermogravimetric Analysis-Mass
9 Spectrometry (TGA-MS), Raman spectroscopy, X-ray Photoelectron Spectroscopy (XPS), X-
10 Ray Diffraction (XRD), Atomic Force Microscopy (AFM) and Transmission Electron
11 Microscopy (TEM). The *grafting from* products showed an increase in the grafting ratio and
12 dispersibility in acetone with increasing monomer supply; on the other hand, due to steric effects,
13 the *grafting to* products showed lower absolute grafting ratios and a decreasing trend with
14 increasing polymer molecular weight. The excellent dispersibility of the *grafting from*
15 functionalised graphene, 900 µg/mL in acetone, indicates an increased compatibility with the
16 solvent and the potential to increase graphene reinforcement performance in nanocomposite
17 applications.

18

19 **Introduction**

20 Graphene related materials are proposed for bulk applications in electronic devices¹,
21 nanocomposites²⁻⁴, supercapacitors⁵ and hydrogen storage⁶, amongst others. Extensive research

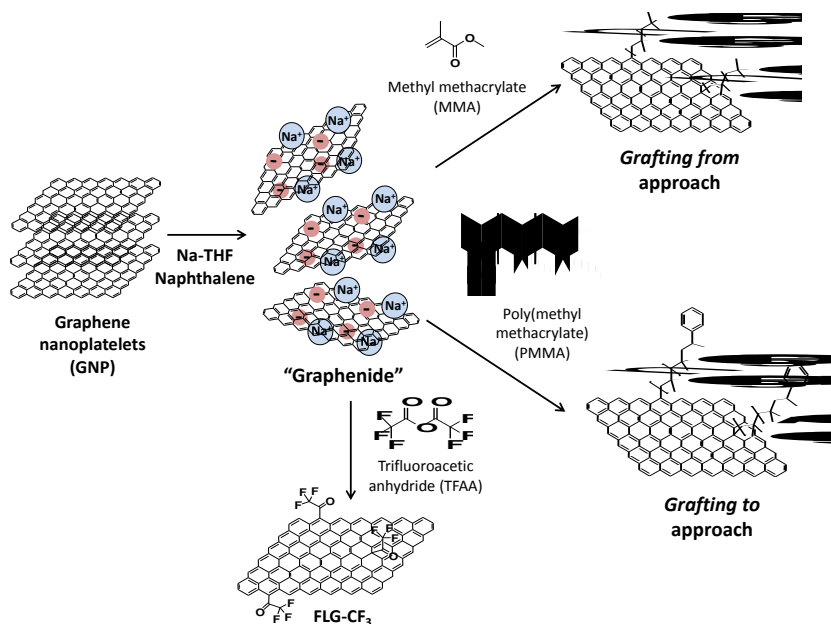
22 is underway in order to improve the compatibility of graphene with processing solvents and
23 polymeric matrices for the preparation of composites^{7, 8}. Covalent functionalisation provides an
24 effective means to adjust the energetics of the surface, as well as to introduce specific steric or
25 electrostatically stabilising moieties. Covalent approaches are more robust than non-covalent
26 alternatives, and avoid any equilibrium with excess free surfactant. These advantages are
27 important in many applications, for example, in the context of composites, where the aim is to
28 enhance the strength of graphene-polymer matrix interfaces. As well as improved compatibility,
29 covalent modification of graphene allows for the stable attachment of groups with specific
30 functional properties (e.g. fluorescent molecules, dopants, etc.)^{9,10}.

31 There are several methods in the literature aiming to produce single layer graphene (SLG) from a
32 variety of starting materials (such as few-layer graphenes (FLGs), natural graphite or graphene
33 nanoplatelets (GNPs)). These methods include liquid-phase¹¹, mechanical¹² or electrochemical
34 exfoliation¹³, among others. Graphite Intercalation Compounds (GICs) are established precursors
35 to produce isolated graphene layers with minimal framework damage¹⁴⁻¹⁶. Exfoliated
36 graphenides can be prepared by various routes, including potassium/liquid ammonia intercalation
37 of graphite¹⁴ and the spontaneous dissolution of potassium-based GICs in N-methyl-2-
38 pyrrolidone (NMP)^{17, 18}. Individual charged graphene sheets can be solvated in dry aprotic
39 solvents, and in one recent case, transferred to water¹⁹. Yet, to stabilise the graphene in other
40 solvents or nanocomposite materials, functional groups are often introduced. The use of
41 covalently grafted polymers is of particular interest for the preparation of nanocomposites²⁰.
42 There are two main approaches to prepare polymer-modified carbon nanomaterials (CNMs):
43 *grafting to* and *grafting from*. The *grafting to* method involves the synthesis of a polymer with a
44 reactive end group that is attached to the surface of the CNM. This method allows explicit

45 control of the molecular weight (M_n) and polydispersity index (PDI). Alternatively, *grafting from*
46 involves *in situ* polymerisation of the monomer directly from the CNM. While the *grafting from*
47 approach promises high grafting ratios, it typically requires the attachment of an initiating group
48 prior to polymerisation²¹⁻²³. *Grafting from* GO (graphite oxide) has been used to grow
49 polystyrene and different methacrylate polymers²². These polymers were grown on the surface of
50 GO using radical polymerisation; however, several preparation steps were involved, including
51 the addition of an alkyne molecule to the GO followed by an azide-terminated chain transfer
52 agent, required to initiate polymerisation. Reductive chemistry provides an alternative method
53 that avoids the use of complex initiators. The formation of polymers in GICs was proposed
54 several decades ago in the investigation of the influence of potassium graphite (KC_8) in the
55 “catalysis” of olefin polymerisation²⁴. The formation of a “graphite-polymer-composite” was
56 described in 1997 where the compound KC_{24} was prepared from highly oriented pyrolytic
57 graphite (HOPG) and reacted with isoprene or styrene vapour at room temperature²⁵. A similar
58 technique was later used in 2006 to produce PMMA-functionalised single-walled nanotubes
59 (SWNTs)²⁶.

60 The dispersibility of polymer-functionalised graphene in a specific solvent should be influenced
61 by the amount of grafted polymer and the distribution of the chains on the graphene surface but
62 these factors are poorly understood. The comparison between *grafting from* and *grafting to*
63 approaches has been described for the functionalisation of carbon nanotubes with polystyrene²⁷,
64 which showed an increase in the dispersibility of the final materials as the grafting ratio
65 increased. A similar study was carried out with graphene oxide²²; in this case, the authors
66 reported an increase in the grafting ratio when using the *grafting from* approach. Here, we
67 explore how the combination of reductive chemistry and different grafting approaches can

68 influence the properties of the final product, such as chain length, grafting ratio, and hence
69 solubility. One of the objectives of this work was to maximise the ambient stability of exfoliated
70 graphene layers in organic solvents with minimal framework damage. PMMA was used as both a
71 classic anionic model system and a potentially relevant system in composite applications, for
72 example to increase dispersibility in epoxies²⁸. The second objective was to compare *grafting to*
73 and *grafting from* approaches as a function of molecular weight to maximise exfoliation and
74 dispersibility.



75
76 **Scheme 1.** Grafting methods used for the functionalisation of graphene sheets with PMMA.

77

78

79

80 **Experimental Section**

81 **Materials**

82 GNPs were provided by Cambridge Nanosystems UK and used without further purification. 1-
83 Bromododecane, dodecane, copper bromide (I) (CuBr), copper bromide (II) (CuBr₂), *N, N, N'*,
84 *N', N'*-pentamethyldiethylenetriamine (PMDETA), (1-bromoethyl)benzene, glacial acetic acid,
85 sodium (99.95%, ingot), naphthalene (99%), poly(methyl methacrylate), trifluoroacetic
86 anhydride and methyl methacrylate were provided by Sigma-Aldrich UK. Naphthalene was dried
87 under vacuum overnight over phosphorus pentoxide (P₂O₅) before using in the glove box. THF
88 was degassed via a freeze-pump-thaw method and dried over 20 % volume molecular sieves 3 Å
89 before use in the glove box. Methyl methacrylate was previously purified by passing the
90 monomer through an alumina column to remove stabilisers and then degassed using the same
91 method as the THF. CuBr was purified by washing with glacial acetic acid, followed by 2-
92 propanol and stored under nitrogen atmosphere.²⁹ In order to carry out the ATRP process,
93 acetone and methyl methacrylate were distilled and stored under nitrogen. Immediately before
94 use both monomer and solvent were purged with nitrogen for 30 min. (1-bromoethyl)benzene
95 and PMDETA were used as received. Holey carbon films on 300 mesh copper grids used for
96 TEM experiments were purchased from Elektron Technology UK Ltd. Aluminium oxide 90
97 active neutral was provided by Merck UK. All gases supplied by BOC, UK.

98 **Polymerisation of PMMA using ATRP**

99 In a typical experiment, CuBr (1.09 mmol, 156.06 mg) and CuBr₂ (0.054 mmol, 12.14 mg) were
100 added to a Schlenk flask, equipped with a stirrer bar, which was previously evacuated and
101 flushed with nitrogen. The flask was degassed and filled with nitrogen three times and then left
102 under nitrogen. Subsequently, methyl methacrylate (54.26 mmol, 6 mL) and acetone (3.12 mL)
103 were added to the flask. PMDETA (1.14 mmol, 238.8 µL) was then added to the reaction
104 mixture and the solution was stirred until the Cu complex was formed. The mixture was

105 degassed using three freeze-pump-thaw cycles. The initiator ((1-bromoethyl)benzene) (1.05
106 mmol, 149.4 μ L) was added after this process and the flask was placed in an oil bath and stirred
107 at 50 °C for different periods of time (30 min, 1 h and 2 h) in order to obtain different molecular
108 weight polymers. The reaction was then stopped by dilution with THF. The solution was filtered
109 through a column filled with neutral aluminium oxide using THF as solvent in order to remove
110 side products. The solvent was evaporated under reduced pressure and the polymer was
111 precipitated in dichloromethane/diethyl ether.

112 $^1\text{H-NMR}$ (CHCl_3 , δ , ppm): 0.77-1.092 (m, 3H, $-\text{CH}_3$), 1.82 (m, 2H, $-\text{CH}_2-$), 3.61 (M, 3H,
113 COOCH_3).

114 GPC (DMF): $M_n = 4977$ g/mol, $\text{Đ} = 1.56$; $M_n = 8039$ g/mol, $\text{Đ} = 1.62$ and $M_n = 9982$ g/mol, $\text{Đ} =$
115 1.65 for 30 minutes, 1 hour and 2 hours reaction time, respectively

116 **Preparation of sodium naphthalide solution**

117 In a typical experiment, 23 mg (1 mmol) of sodium and 128 mg (1 mmol) of dried naphthalene
118 were dissolved in 10 mL of degassed anhydrous THF in a nitrogen filled glove box, and stirred
119 using a glass stirrer for two hours forming a green sodium-naphthalene solution.

120 **Exfoliated graphene**

121 In a typical experiment, starting material GNP (15 mg) and a glass magnetic bar were placed in a
122 Schlenk tube and flame-dried at 400°C under vacuum. The Schlenk tube was placed in the glove
123 box. 1.04 mL of the sodium naphthalide solution were added to the graphene followed by 11.46
124 mL of degassed THF (C:Na ratio used was 12, which corresponds to a sodium concentration of
125 0.01 M).¹⁵ The suspension was stirred for 24 hours. After this period of time, dry N_2/O_2 80/20

126

127 was bubbled into the solution for 15 minutes, the solution was stirred for 1 day under N₂/O₂
128 80/20 vol% for oxidation of any remaining charges on the graphene¹⁵. Subsequently, the
129 graphene was filtered through a 0.2 μm PTFE filter membrane and washed thoroughly with
130 THF, water and ethanol.

131 **Functionalisation of graphene with trifluoroacetic anhydride (TFAA)**

132 In a typical experiment, starting material GNP (15 mg) and a glass magnetic bar were placed in a
133 Schlenk tube and flame-dried at 400°C under vacuum. The Schlenk tube was placed in the glove
134 box. 1.04 mL of the Na-naphthalene solution were added to the graphene followed by 11.46 mL
135 of degassed THF. The suspension was stirred for 24 hours. After this period of time, the reaction
136 was sealed and transferred outside the glove box and previously degassed TFAA (0.31 mmol,
137 44.07 μL) were added to the reaction mixture. The solution was allowed to stir for 24 hours.
138 After this period of time, dry N₂/O₂ 80/20 vol% was bubbled into the solution for 15 minutes, the
139 solution was stirred for 1 day under N₂/O₂ 80/20 for oxidation of any remaining charges on the
140 graphene. The graphene was then filtered through a 0.2 μm PTFE filter membrane and washed
141 thoroughly with THF, water and ethanol.

142 **PMMA functionalised graphene using the *grafting from* approach**

143 In a typical experiment, starting material GNP (15 mg) and a glass magnetic bar were placed in a
144 Schlenk tube and flame-dried at 400°C under vacuum. The Schlenk tube was placed in the glove
145 box. 1.04 mL of the Na-naphthalene solution were added to the graphene followed by 11.46 mL
146 of degassed THF. The suspension was stirred for 24 hours. After this period of time, the reaction

147 was sealed and transferred outside the glove box and different amounts of previously degassed
148 methyl methacrylate (1.56 mmol, 162 μL ($M_n = 800$ g/mol), 3.12 mmol, 337 μL ($M_n = 1000$
149 g/mol), 6.24 mmol, 674 μL ($M_n = 1400$ g/mol), 9.36 mmol, 1.035 mL ($M_n = 2300$ g/mol)) were
150 added to the reaction mixture. The solution was allowed to stir for 24 hours. After this period of
151 time, dry N_2/O_2 80/20 vol% was bubbled into the solution for 15 minutes, the solution was
152 stirred for 1 day under N_2/O_2 80/20 for oxidation of any remaining charges on the graphene. The
153 graphene was then filtered through a 0.2 μm PTFE filter membrane and washed thoroughly with
154 THF, acetone, water and ethanol.

155 **PMMA functionalised graphene using *grafting to* approach**

156 In a typical experiment, starting material GNP (15 mg) and a glass magnetic bar were placed in a
157 Schlenk tube and flame-dried at 400°C under vacuum. The Schlenk tube was placed in the glove
158 box. 1.04 mL of the Na-naphthalene solution (1:1 in THF) were added to the graphene followed
159 by 11.46 mL of degassed THF. The suspension was stirred for 24 hours. After this period of
160 time, different amounts of brominated PMMA (0.104 mmol, 520 mg ($M_n = 5000$ g/mol), 0.104
161 mmol, 832 mg ($M_n = 8000$ g/mol), 0.104 mmol, 1.04 g ($M_n = 10000$ g/mol)) were added to the
162 reaction mixture. The solution was allowed to stir for 24 hours. After this period of time, dry
163 N_2/O_2 80/20 was bubbled into the solution for 15 minutes, the solution was stirred for 1 day
164 under N_2/O_2 80/20 vol% for oxidation of any remaining charges on the graphene. The graphene
165 was then filtered through a 0.2 μm PTFE filter membrane and washed thoroughly with THF,
166 acetone, water and ethanol.

167 **Measurements**

168 TGA was performed using a METTLER Toledo TGA-DSC 1 integrated with a Hiden HPR-20
169 QIC EGA mass spectrometer under a N₂ atmosphere. Samples were held at 100°C for 30 min
170 under N₂ flow of 60 ml/min, then ramped at 10°C/min to 800°C. XRD measurements were
171 carried out using dried powder samples. Data were processed using Polymer Labs Cirrus
172 software. These samples were loaded onto zero-background XRD sample holders. The
173 measurement was recorded at a scan rate of 0.108°/s with the Cu K α (1.542 Å) line using a
174 PANalytical X'Pert PRO diffractometer. Polymer M_n were assessed using a Polymer Labs GPC
175 50 system with two PL-gel 5 μ columns. Samples were eluted with dimethylformamide (DMF)
176 with 1% triethylamine (TEA) and 1% acetic acid. The instrument was calibrated to PMMA
177 standards. All XPS spectra were recorded using a K-alpha⁺ XPS spectrometer equipped with a
178 MXR3 Al K α monochromated X-ray source (h ν = 1486.6 eV). X-ray gun power was set to 72 W
179 (6 mA and 12 kV). Charge compensation was achieved using the FG03 flood gun using a
180 combination of low energy electrons and the ion flood source. Argon etching of the samples was
181 done using the standard EX06 Argon ion source using 500 V accelerating voltage and 1 μ A ion
182 gun current. Survey scans were acquired using 200 eV pass energy, 1 eV step size and 100 ms
183 (50 ms x 2 scans) dwell times. All high resolution spectra (C1s, and O1s) were acquired using 20
184 eV pass energy, 0.1 eV step size and 1 second (50ms x 20 scans = 1000 ms) dwell times.
185 Samples were prepared by pressing the sample onto double side sticky carbon based tape.
186 Pressure during the measurement of XPS spectra was $\leq 1 \times 10^{-8}$ mbar. Thermo Advantage
187 software was used for data interpretation. Casa XPS software (version 2.3.16) was used to
188 process the data. The quantification analysis was carried out after subtracting the baseline using
189 the Shirley or two point linear background type. Peaks were fitted using GL(30) lineshapes; a
190 combination of Gaussian (70%) and Lorentzian (30%). All XPS spectra were charge corrected

191 by referencing the fitted contribution of C-C graphitic like carbon in the C1s signal 284.5 eV.
192 UV-vis-NIR absorption spectra were measured using a Perkin Elmer Lambda 950 UV-vis
193 spectrometer in the range of wavelengths between 800 and 400 nm. A quartz cuvette with 1 cm
194 pathlength was used for these measurements. Raman spectra of powder samples were measured
195 using a Renishaw in Via confocal Raman spectrometer equipped with a 532 nm excitation laser
196 source; mapping measurements were carried out using the Streamline mode (between 500 – 1000
197 spectra over at least 3 different areas). Samples were prepared by drop casting graphene
198 dispersions on a glass slide. The exposure time was 10 s with a laser intensity of 3.2 mW and
199 grating 1800 l/mm. Data were analysed using Wire 4.1 and OriginPro 9. The D peak was fitted
200 by one Gaussian function, and the G and 2D peaks were fitted using a mixture of Lorentz and
201 Gaussian functions. Tapping-mode atomic force microscopy (AFM) measurements were taken
202 using Bruker MultiMode 8 AFM. Samples for AFM were prepared by drop-casting dilute
203 dispersed-graphene chloroform solutions on silica substrates. ¹H-NMR measurements were
204 carried out using a Bruker NM 400 spectrometer operating at 9.4 T. Samples were dissolved in
205 Deuterated chloroform (CDCl₃) and all spectra were recorded with 16 scans. All chemical shifts
206 (δ) are given in ppm, where the residual CHCl₃ peak was used as an internal reference ($\delta = 7.28$
207 ppm). TEM was carried out using a JEOL2100Plus TEM at 200 kV operating voltage. One drop
208 of the graphene solution in acetone (100 μ g/mL) was deposited on a TEM grid and allowed to
209 evaporate at room temperature. The TEM grid was subsequently kept under vacuum overnight
210 before the measurement. The measurements of adsorption and desorption isotherms of nitrogen
211 at 77 K were carried out on 20 mg-50 mg of FLG using a Micromeritics ASAP 2010 apparatus.
212 Specific surface areas were calculated according to the Brunauer, Emmett and Teller (BET)

213 equation from the adsorption isotherms in the relative pressure range of 0.05 p/p₀–0.20 p/p₀.
214 Prior to analysis, the samples were degassed with continuous N₂ flow at 100 °C for 12 hours.

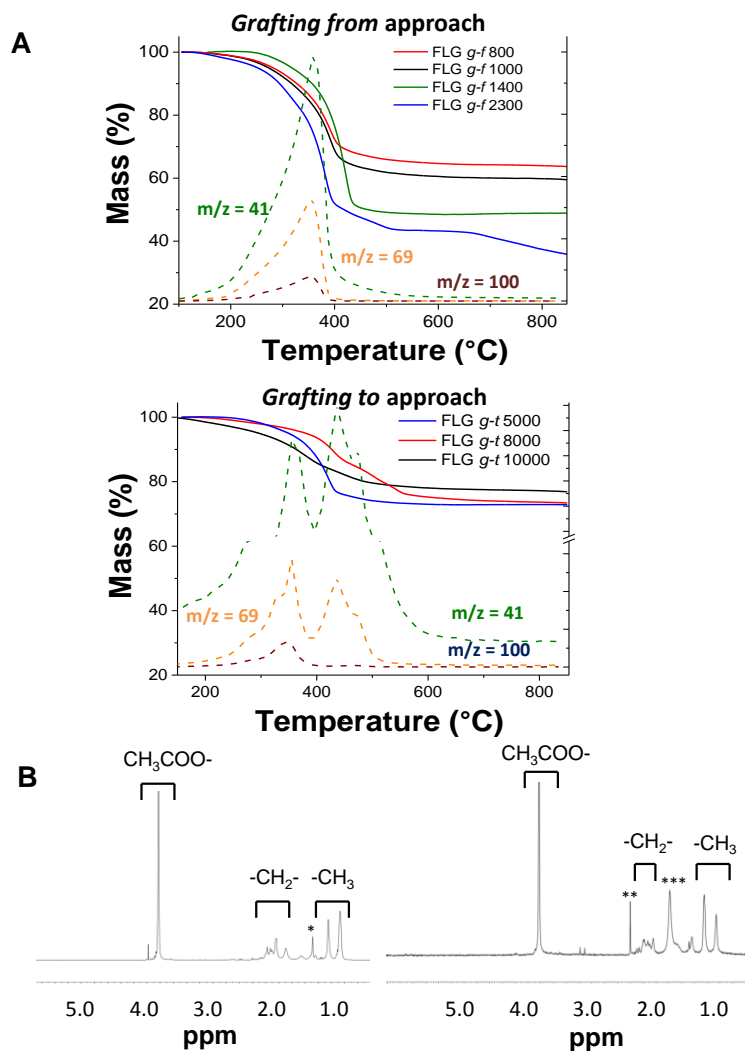
215

216 **Results and discussion**

217 The selected starting material was a type of GNP grown by chemical vapour deposition (CVD);
218 it provides a relatively crystalline framework by a simple one step synthesis, whilst offering high
219 exfoliation yields in subsequent reactions. The exfoliation of the GNP starting material was
220 carried out using a standard methodology developed for grafting short alkyl groups^{15, 30}: sodium
221 and naphthalene were used as the reducing agent and transfer reagent (**Scheme 1**), respectively.
222 Tetrahydrofuran (THF) was used as the solvent due to its ability to coordinate sodium ions³¹.
223 PMMA was grafted from the graphenide by adding methyl methacrylate (MMA) monomer to the
224 chemically reduced graphene solution. GNP was exfoliated into FLG using a C/sodium ratio of
225 12 reported previously¹⁵, based on an optimum value found to balance the need to charge the
226 graphenide with the tendency for charge condensation. Sodium/MMA ratios of 1:15, 1:30, 1:60
227 and 1:90 were used in order to grow polymers of different molecular weights. The resulting
228 GNP-PMMA products were characterised using TGA-MS under nitrogen. The GNP starting
229 material shows a small mass loss (2.8 wt%) in the range from 100 °C to 800 °C (**Figure S1A**),
230 probably due to the decomposition of organic impurities or oxygen functionalities, while the
231 exfoliated sample (Na-reduced FLG) shows a mass loss (13.8 wt%) related to the presence of
232 THF molecules in the sample (m/z = 41, **Figure S1B**). TGA-MS of PMMA-grafted FLG
233 samples prepared using the *grafting from* approach (**Figure 1A** top panel) show the expected
234 PMMA fragments (m/z = 69 and m/z = 100) evolved in the same temperature range on which

235 pure PMMA homopolymer fully decomposes (**Figure S3**). However, the $m/z = 41$ peak indicates
236 the presence of some solvent molecules within the graphene layers after the reaction, suggesting
237 the formation of stage-1 Na-THF-GICs complexes^{15,31}. In order to quantify the ratio of trapped
238 solvent and grafted PMMA on the graphene layers, the relative mass fractions of each
239 component were estimated from the MS peaks (**Figure S2** and **Table S1** for more details).
240 Controls were prepared by mixing either MMA or PMMA-Br ($M_n \sim 5000$ g/mol) with quenched
241 Na-reduced FLG (ESI); in both cases, TGA-MS after work-up (**Figure S6A-B**) showed no
242 MMA-related signals, ruling out physisorption of either monomer or polymer. Grafting ratio is
243 defined as the weight percentage of covalently attached polymer relative to the graphitic carbon.
244 High grafting ratios were obtained using the *grafting from* approach (44.6% - 126.5%, **Table 1**).
245 There are actually a number of active sites which are expected to be determined by the number
246 of charges and is only a fraction of the total charge introduced^{32,33}. In order to estimate the
247 number of active sites initiating the polymerisation, the graphenide was functionalised with
248 trifluoroacetic anhydride (TFAA) (**Scheme 1**). This molecule is a similar size and contains a
249 trifluoromethyl group that can be detected using TGA-MS and XPS; whilst the reactivities of
250 TFAA and MMA may not be the identical, any variation will generate only a relative shift of
251 otherwise consistent grafting trends. Both techniques (**Figure S5**) quantified the fluorine-
252 containing groups grafted on the layers (one group every 149 carbon atoms from XPS
253 calculations), and hence indicate the efficiency of the grafting reaction (**Table S2**). Raman
254 spectroscopy (**Figure S5**) also confirmed the introduction of these functional groups. The M_n of
255 the grafted polymer was estimated from the grafting ratio, by assuming the same density of
256 active sites (**Table S1**). The values varied from 800 g/mol up to 2300 g/mol, increasing as
257 expected with MMA:Na ratio.

258 Bromine-terminated PMMA polymers with different M_n were prepared for the *grafting to*
259 approach, using Atom Transfer Radical Polymerisation (ATRP), following a previous protocol²⁹.
260 The polymerisation process was carried out varying the reaction times in order to obtain
261 polymers with different M_n in the range from 5000 to 10000 g/mol. As noted above, a simple
262 mixing control excludes possible physisorption. The negative charges on the graphene surface
263 react with the bromine-terminated polymer (electrophile), to form the products FLG-*g-t* 5000,
264 FLG-*g-t* 8000 and FLG-*g-t* 10000. TGA-MS analysis (**Figure 1A** bottom panel) shows typical
265 PMMA fragments for all the grafted samples ($m/z = 69$ and $m/z = 100$). Mass loss values were
266 extracted from the TGA graphs taking into account the amount of trapped solvent (**Table 1**).
267 Grafting ratio decreases as the M_n of the grafted polymer increases (from 20.3% down to 12.6%,
268 for FLG-*g-t* 5000 and FLG-*g-t* 10000, respectively), likely due to increased steric hindrance as
269 discussed.



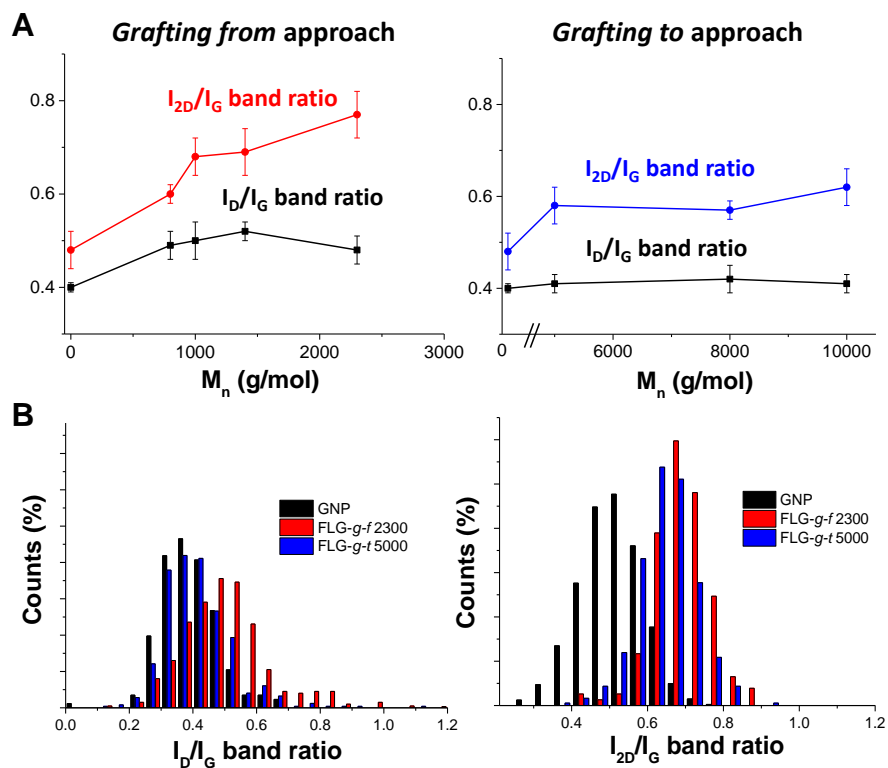
270
 271 **Figure 1.** Characterisation of PMMA-grafted GNP. (A) TGA-MS of the PMMA-grafted GNP
 272 using *grafting from* (top panel) and *grafting to* approaches (bottom panel). MS fragments
 273 correspond to $\text{CH}_2=\text{CH-CH}_2^+$ ($m/z = 41$), $\text{CH}_2=\text{C}=\text{C-O-CH}_3^+$ ($m/z = 69$) and $\text{CH}_2=\text{CH-CO-O-}$
 274 CH_3^+ ($m/z = 100$). (B) $^1\text{H-NMR}$ spectra of commercial PMMA polymer (left panel) and FLG-*g-f*
 275 1400 (right panel).*, ** and *** indicate the presence of residual tetrahydrofuran, acetone and
 276 water, respectively.

277 The $^1\text{H-NMR}$ spectrum of commercial PMMA shows the typical signals from the polymer
 278 (**Figure 1B** left panel). The peak at 3.6 ppm corresponds to the protons from COOCH_3 in each

279 MMA unit. The peaks observed at 0.89 ppm and 1.09 ppm correspond to the CH₃ groups, while
280 the peaks at 1.57 ppm are attributed to the CH₂ groups. These peaks can be observed in the
281 spectrum from FLG-*g-f* 1400 (**Figure 1B** right panel), confirming the presence of polymer on the
282 graphene layers. Polymer signals were also observed for the sample FLG-*g-f* 2300 (**Figure S7**);
283 however, these signals were very weak for the sample FLG-*g-f* 1000, probably due to the lower
284 polymer content and hence, dispersibility (see below). Similarly, measurable NMR peaks were
285 weaker for the *grafting to* samples.

286 Raman spectroscopy provided quantitative data about the ratios of the D and G bands and 2D
287 and G bands obtained from statistical mapping experiments (I_D/I_G and I_{2D}/I_G respectively)
288 (**Figure 2**). Mean I_D/I_G values of 0.52 ± 0.02 for the *grafting from* approach showed an increase
289 compared to the GNP starting material (I_D/I_G 0.40 ± 0.02 , **Figure S8A**), suggesting an increase in
290 the number of sp³ atoms due to the presence of grafting sites after the polymerisation process.
291 The much lower I_D/I_G values of 0.42 ± 0.03 displayed by the *grafting to* products are not
292 significantly greater than the Na-reduced control sample. This result is not surprising since the
293 grafting density for the *grafting to* approach is an order of magnitude lower compared to the
294 *grafting from* approach (**Table 1**), due to the steric bulk of the polymers. The ratio of the 2D
295 band and G band (I_{2D}/I_G) averages 0.49 ± 0.03 for GNP starting material; an increase in this ratio
296 indicates the presence of a higher proportion of SLG in the sample. A value of I_{2D}/I_G up to $0.59 \pm$
297 0.04 was observed for the Na-reduced FLG (**Figure S8B**), suggesting an increase in the degree
298 of exfoliation. Higher I_{2D}/I_G ratios for PMMA grafted samples indicate greater exfoliation of the
299 graphene layers after the functionalization. This increase in the I_{2D}/I_G ratios was larger for the
300 *grafting from* approach (up to 0.77 ± 0.05) compared to the *grafting to* approach (0.62 ± 0.02).
301 These samples show a high intensity and symmetrical 2D band, this shape suggests the existence

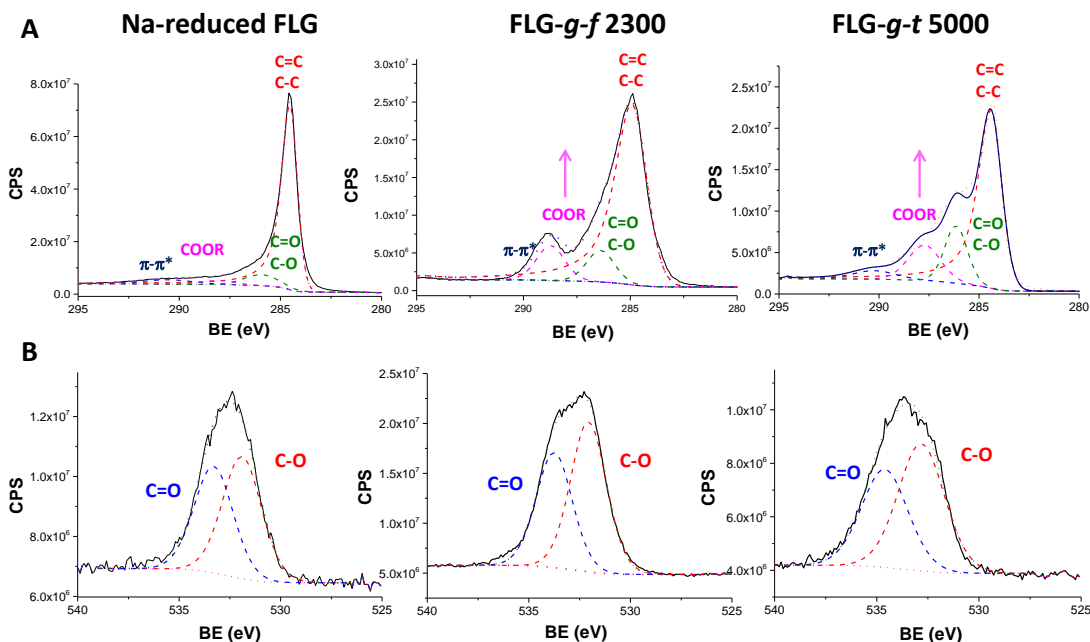
302 of single-layer and/or few layer graphene³⁴. The full width at half maximum of the 2D band
 303 (FWHM_{2D}) did not change significantly between samples (**Table S5**), and is typical of
 304 chemically exfoliated FLG³⁵.



305
 306 **Figure 2.** (A) Average I_D/I_G and I_{2D}/I_G ratios of FLG-PMMA obtained using *grafting from* and
 307 *grafting to* approaches and (B) I_D/I_G and I_{2D}/I_G histograms of FLG-*g-f* 2300 and FLG-*f-t* 5000
 308 representative samples of both approaches.

309 C1s XPS spectra of Na-reduced FLG, FLG-*g-f* 2800 and FLG-*g-t* 5000 samples (**Figure 3A**)
 310 were deconvoluted into different bands: C=C and C-C (284.5 eV), C-O and C=O (286.4 eV),
 311 COOR (288.7 eV) and the π - π^* transition (290.7 eV) (See **Table 1** for quantitative data of all the
 312 samples). Similar components are observed for Na-reduced FLG and for the GNP starting
 313 material (**Figure S9**), suggesting that the exfoliation process does not itself introduce a large

314 number of additional oxygen functionalities on the graphene layers. The slight increase in the
315 absolute amount of oxygen after the exfoliation process (from 4% to 5%) could be due to the
316 presence of trapped solvent within the layers (**Table 1**). On the other hand, when carrying out the
317 reaction using the *grafting from* and *grafting to* approaches, a significant increase in the COO-
318 band appears, together with a broadening of the C=C/C-C band due to an increase in the number
319 of C-C bonds and a higher contribution from the C=O band. The oxygen and carbon atomic
320 percentages change very significantly after introducing the different polymers (**Table 1**). FLG-*g-*
321 *f*2300 has an oxygen content of 23.5% while FLG-*g-t* 5000 sample shows a lower value of
322 9.58%, consistent with a lower degree of functionalisation for the *grafting to* approach. The
323 grafting density (expressed as number of graphene carbon atoms per polymer chain) obtained
324 from XPS values is in good agreement with the results obtained from TGA values, after
325 subtracting the excess solvent still trapped within the graphene layers (**Table 1**). For the samples
326 obtained using the *grafting from* approach, the grafting density found from XPS varied between
327 150 and 340, which is close to the value obtained from TGA calculations (one functional group
328 every 149 carbon atoms). The low sodium content found in the samples ($0.11\% \pm 0.02\%$)
329 indicates that the majority of the metal used for the exfoliation was removed by washing.
330 Deconvolution of the O1s spectrum (**Figure 3B**) results in two different peaks, O-C (532.05 eV)
331 and O=C (533.4 eV), related to PMMA, which are similar for the grafted samples.

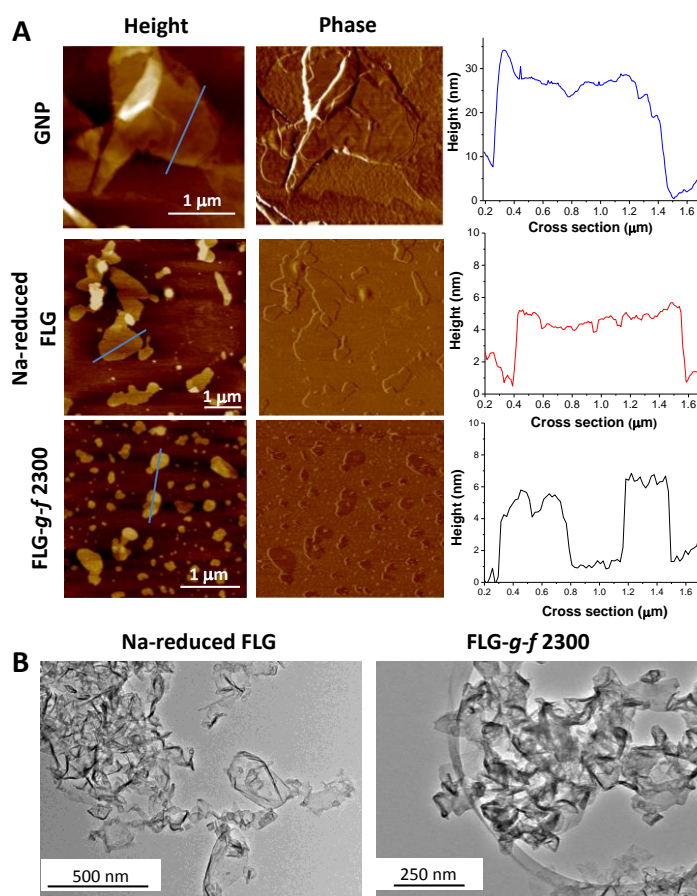


332

333 **Figure 3.** Deconvoluted XPS spectra of the (A) C1s and (B) O1s regions obtained from Na-
 334 reduced FLG (left panels), FLG-*g-f* 2300 (middle panels) and FLG-*g-t* 5000 (right panels). These
 335 samples were chosen as representative examples of both grafting approaches.

336 XRD measurements provide information about the interlayer distance (d) using Bragg's law and
 337 the number of stacked layers (N) using the Scherrer equation³⁶. X-ray diffractograms (**Figure**
 338 **S10**) of the different graphene-polymer samples show the typical graphite (002) peak at a 2θ
 339 value of 26.2° . The weak diffraction pattern of the GNP starting material (**Figure S10**, left panel)
 340 suggests that the graphene layers of the initial material are partially exfoliated. After the
 341 polymerisation process, a broadening of the (002) peak is observed for all samples, indicating
 342 successful further exfoliation of the FLG material³⁷. The average number of layers was 41 for the
 343 GNP starting material (**Table S6**) and 16 for the Na-reduced FLG. After functionalisation with
 344 PMMA, the number of layers per stack decreased to an average of 6 and 9 layers for the *grafting*
 345 *from* and *grafting to* method, respectively.

346 The morphology and degree of exfoliation of the FLG-PMMA were assessed using Atomic
 347 Force Microscopy (AFM) and Transmission Electron Microscopy (TEM) (**Figure 4**). AFM
 348 images of GNP starting material show agglomerated flakes with heights between 20.6 ± 5.5 nm,
 349 corresponding to an average of 61 layers. Na-reduced FLG shows a lateral size of 639.9 nm \pm
 350 171.4 nm. The presence of few-layer graphene in this sample indicates successful exfoliation of
 351 the starting material (average height: 4.4 nm \pm 0.61 nm). FLG-*g-f* 2300 shows a better degree of
 352 exfoliation, the average height in this case is 3.1 nm \pm 0.4 nm, in good agreement with the results
 353 obtained from XRD measurements; the average number of layers significantly decreased after
 354 functionalisation with PMMA.



355
 356 **Figure 4.** AFM images (A) of GNP starting material, Na-reduced FLG and FLG-*g-f* 2300. TEM
 357 images (B) Na-reduced FLG and FLG-*g-f* 2300.

358 **Table 1.** Summary of grafting analysis data for FLG-PMMA samples

Sample	Grafting ratio (%)	Dispersibility (mg/mL)	Grafting density ^a	Grafting density ^b	C (%) ^b	O (%) ^b	Surface concentration of grafted PMMA ($\mu\text{mol m}^{-2}$) ^a	PMMA separation <i>D</i> (nm)	<i>R_F</i> (nm)
GNP	-	3.8	-	-	95.9	3.91	-	-	-
Na-reduced FLG	-	530	-	-	94.3	5.22	-	-	-
FLG- <i>g-f</i> 800	44.6	720	149	278	89.7	9.9	0.85	1.6	1.8
FLG- <i>g-f</i> 1000	55.6	760	149	334	89.2	10.1	0.80	1.6	2.1
FLG- <i>g-f</i> 1400	79.1	875	149	151	79.6	20.2	0.65	1.8	2.6
FLG- <i>g-f</i> 2300	126.5	920	149	208	75.6	23.5	0.50	2.1	5.0
FLG- <i>g-t</i> 5000	20.3	670	2055	1869	89.7	10.0	0.07	5.5	5.8
FLG- <i>g-t</i> 8000	15.1	650	4421	4390	90.9	9.0	0.03	8.0	7.7
FLG- <i>g-t</i> 10000	12.6	710	6615	5490	91.6	8.2	0.02	9.5	8.8

^a Values obtained from TGA calculations. ^b Values obtained from XPS calculations.

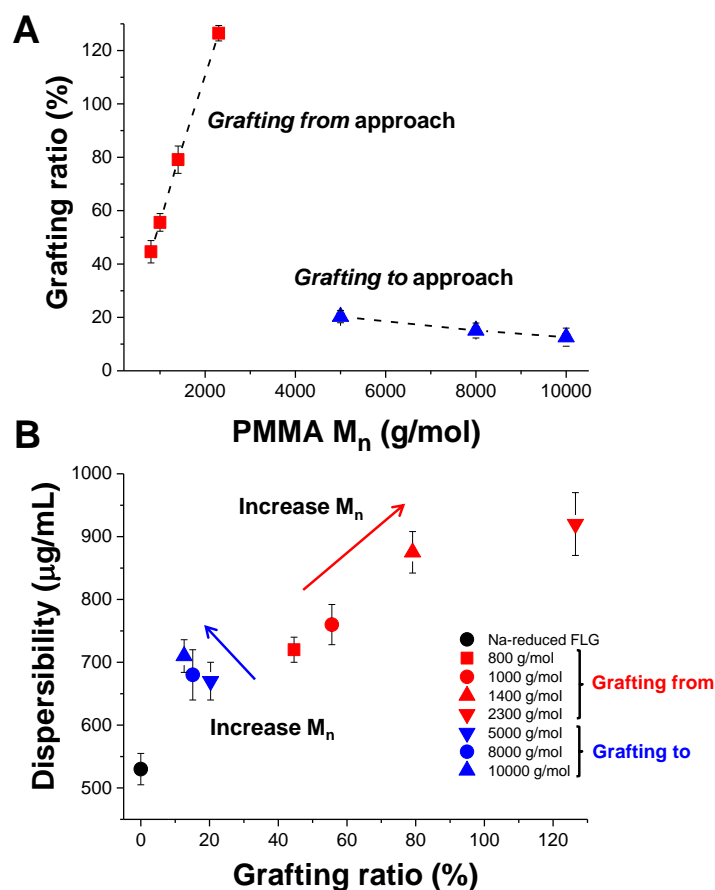
359

360 TEM images (**Figure 4B**) of Na-reduced FLG and FLG-*g-f* 2800 show a similar morphology to
 361 the starting material (**Figure S11**), suggesting that the exfoliation/functionalisation procedure did
 362 not damage the graphene sheets. The lateral sizes for individual graphene sheets are in the range
 363 between 200 and 500 nm, with no significant differences observed after functionalisation.

364 Overall, the TGA-MS and XPS data indicate that PMMA polymer was successfully introduced
 365 on the graphene surface by both *grafting from* and *grafting to* methods. Both the grafting ratio
 366 and the grafting density were higher for the *graft from* reactions (**Table 1**). Raman and XRD data
 367 suggest that a much greater degree of exfoliation was achieved by the *grafting from* method,
 368 which is also supported by AFM observations.

369 The grafting ratio trend of the *grafting from* products shows an increase from 44.6% (FLG-*g-f*
 370 1100) up to 126.5% (FLG-*g-f* 2300) as the M_n increases (**Figure 5A**); a similar trend was
 371 reported, for the functionalisation of carbon nanotubes with polystyrene grown by ATRP²⁷.
 372 However, the estimated M_n values obtained for the FLG-*g-f* products were lower than reported

373 for the ring opening polymerisation of caprolactam on oxidised carbon nanotubes³⁸ (estimated
374 1280 - 8480 g/mol). On the other hand, the *grafting to* products show the opposite trend in
375 grafting ratios, compared to the *grafting from* approach (**Figure 5A**), most likely due to steric
376 hindrance. Once a polymer chain grafts on the graphene surface, its volume occludes a large area
377 of that surface, preventing grafting of another chain nearby. The grafting ratio of polystyrene-
378 grafted to SWNTs was also reported to decrease with M_n ³⁹. For each of the FLG products, the
379 surface concentration of grafted polymer and average PMMA chain separation, D , were
380 estimated using the Na-reduced FLG specific surface area ($420.08 \text{ m}^2/\text{g} \pm 4.51 \text{ m}^2/\text{g}$) (**Table 1**
381 and **Table S5**)³⁰. The conformation of the grafted PMMA polymer can be predicted from the
382 average separation, D , between grafting sites. The estimated spacings ranged between 1.6 and
383 2.1 nm for the *grafting from* products; this value is below the theoretical values of the Flory
384 radius (obtained using $R_F = M^{3/5}a$, where a is the repeat length and M the number of monomers
385 per chain)⁴⁰ for all the samples. According to de Gennes' model⁴⁰, this trend suggests that the
386 polymers must therefore grow in a brush-like fashion. Adjusting the estimates to account for the
387 observed degree of exfoliation does not change the expected conformation (see ESI for more
388 information). The *grafting to* approach shows D values in the range between 5.5 nm and 9.5 nm
389 for polymer chains between 5000 and 10000 g/mol. These values are similar to or larger than the
390 calculated R_F values (between 5.8 nm and 8.8 nm), suggesting that the polymer follows a
391 mushroom regime in this case, where the polymer chains coil. These changes in regime are
392 consistent with the grafting ratio trends and the proposed mechanisms.



393
 394 **Figure 5.** Grafting density and dispersibility plots of PMMA grafted FLG using the *grafting*
 395 *from* and *grafting to* approaches.

396 The dispersibility of PMMA-grafted FLG in acetone was quantified using UV-vis spectroscopy.
 397 A known mass was sonicated in acetone for five minutes, allowed to sediment overnight, and the
 398 supernatant concentrations measured using the extinction coefficient¹¹ of graphene in solution
 399 ($\alpha_{660} = 2460 \text{ L/g m}$). The dispersibility of GNP starting material was low (3.8 µg/ml) (**Figure**
 400 **S12**) but increased remarkably for Na-reduced FLG (530 µg/ml) and polymer modified
 401 graphene, by 250 times for FLG-*g-f* 1400 (920 µg/ml) and 170 times for FLG-*g-t* 5000 (650
 402 µg/ml). The trend according to the grafting ratios shows an increase in the dispersibility of the
 403 material as the grafting ratio increases for the *grafting from* approach (**Figure 5** bottom panel).

404 On the other hand, the dispersibility behaviour remained the same for the different materials
405 obtained from the *grafting to* approach. These values are higher than values reported in the
406 literature for reduced-GO-PMMA with different M_n polymers attached to the graphene layers,
407 150 $\mu\text{g/ml}$ and 140 $\mu\text{g/ml}$ for graphene-PMMA *g-f* 10000 and graphene-PMMA *g-t* 5000,
408 respectively,²² with grafting ratios of 49.3% and 50.7%, respectively. Improved grafting ratio
409 and dispersibility results in the present study are very promising for the incorporation of PMMA-
410 grafted FLG into different matrices.

411 **Conclusion**

412 In conclusion, reductive chemistry provides a route to functionalise graphene with PMMA
413 polymers via both *grafting to* and *grafting from* approaches. Direct anionic polymerisation using
414 graphenide as an initiator was particularly effective for grafting PMMA in situ, without the need
415 of introducing specific initiator groups. The grafting ratio was high and systematically controlled
416 by monomer addition. The solubility in acetone of the *grafting from* products is directly related
417 to the M_n and grafting ratios (**Figure 5**), with an increase in the solubility when increasing M_n ;
418 however, it is not straight forward to measure the M_n of the polymer attached on the surface of
419 the graphene. On the other hand, while there is perfect control of the polymer M_n when using the
420 *grafting to* approach, the solubility and grafting ratios obtained are lower compared to the
421 *grafting from* approach. The use of reductive chemistry for *in situ* polymerization should allow
422 the introduction of block polymers and other variants in the future. This approach should also be
423 applicable to a range of graphitic starting materials including natural graphite, synthetic graphite
424 or FLG. The final polymer-graphene hybrids could be used in a wide range of applications, such
425 as sensors, as electrodes in energy storage materials, biomedical materials and in coatings for
426 fuselages.

427 ASSOCIATED CONTENT

428 **Data statement**

429 Supporting data can be requested from the corresponding author, but may be subject to
430 confidentiality obligations.

431 AUTHOR INFORMATION

432 **Corresponding Author**

433 *m.shaffer@imperial.ac.uk

434 **Author Contributions**

435 ‡ Equal contribution

436 **Notes**

437 The authors declare no competing financial interests.

438

439 ACKNOWLEDGMENT

440 We are grateful to Dr. Ignacio Villar-García (Imperial College London) for discussions in
441 interpreting XPS spectra. Funding from Engineering and Physical Sciences Research Council
442 (EPSRC/EP/K016792/1 and EP/K01658X/1) is also acknowledged. We are also grateful to
443 Catharina Paukner (FGV Cambridge Nanosystems Limited) for providing the GNP starting
444 material.

445

446

447

- 449 1. Zhang, J. S.; Chen, Y.; Wang, X. C. Two-dimensional covalent carbon nitride
450 nanosheets: synthesis, functionalization, and applications. *Energ Environ Sci* **2015**, 8 (11), 3092-
451 3108 DOI: 10.1039/c5ee01895a.
- 452 2. Wang, F. Z.; Drzal, L. T.; Qin, Y.; Huang, Z. X. Mechanical properties and thermal
453 conductivity of graphene nanoplatelet/epoxy composites. *J Mater Sci* **2015**, 50 (3), 1082-1093
454 DOI: 10.1007/s10853-014-8665-6.
- 455 3. Das, B.; Eswar Prasad, K.; Ramamurty, U.; Rao, C. N. Nano-indentation studies on
456 polymer matrix composites reinforced by few-layer graphene. *Nanotechnology* **2009**, 20 (12),
457 125705 DOI: 10.1088/0957-4484/20/12/125705.
- 458 4. Jung, H.; Yu, S.; Bae, N. S.; Cho, S. M.; Kim, R. H.; Cho, S. H.; Hwang, I.; Jeong, B.;
459 Ryu, J. S.; Hwang, J.; Hong, S. M.; Koo, C. M.; Park, C. High through-plane thermal conduction
460 of graphene nanoflake filled polymer composites melt-processed in an L-shape kinked tube. *ACS*
461 *applied materials & interfaces* **2015**, 7 (28), 15256-62 DOI: 10.1021/acsami.5b02681.
- 462 5. Liu, C. G.; Yu, Z. N.; Neff, D.; Zhamu, A.; Jang, B. Z. Graphene-Based Supercapacitor
463 with an Ultrahigh Energy Density. *Nano Lett* **2010**, 10 (12), 4863-4868 DOI:
464 10.1021/nl102661q.
- 465 6. Tozzini, V.; Pellegrini, V. Prospects for hydrogen storage in graphene. *Phys Chem Chem*
466 *Phys* **2013**, 15 (1), 80-89 DOI: 10.1039/c2cp42538f.
- 467 7. Ahmadi-Moghadam, B.; Sharafimasooleh, M.; Shadlou, S.; Taheri, F. Effect of
468 functionalization of graphene nanoplatelets on the mechanical response of graphene/epoxy
469 composites. *Mater Design* **2015**, 66, 142-149 DOI: 10.1016/j.matdes.2014.10.047.
- 470 8. Tang, L. C.; Wan, Y. J.; Yan, D.; Pei, Y. B.; Zhao, L.; Li, Y. B.; Wu, L. B.; Jiang, J. X.;
471 Lai, G. Q. The effect of graphene dispersion on the mechanical properties of graphene/epoxy
472 composites. *Carbon* **2013**, 60, 16-27 DOI: 10.1016/j.carbon.2013.03.050.
- 473 9. Gatti, T.; Vicentini, N.; Mba, M.; Menna, E. Organic Functionalized Carbon
474 Nanostructures for Functional Polymer-Based Nanocomposites. *Eur J Org Chem* **2016**, (6),
475 1071-1090 DOI: 10.1002/ejoc.201501411.
- 476 10. Liu, J. W.; Ye, Y. S.; Xue, Y.; Xie, X. L.; Mai, Y. W. Recent Advances in Covalent
477 Functionalization of Carbon Nanomaterials with Polymers: Strategies and Perspectives. *J Polym*
478 *Sci Pol Chem* **2017**, 55 (4), 622-631 DOI: 10.1002/pola.28426.
- 479 11. Hernandez, Y.; Nicolosi, V.; Lotya, M.; Blighe, F. M.; Sun, Z. Y.; De, S.; McGovern, I.
480 T.; Holland, B.; Byrne, M.; Gun'ko, Y. K.; Boland, J. J.; Niraj, P.; Duesberg, G.; Krishnamurthy,
481 S.; Goodhue, R.; Hutchison, J.; Scardaci, V.; Ferrari, A. C.; Coleman, J. N. High-yield
482 production of graphene by liquid-phase exfoliation of graphite. *Nat Nanotechnol* **2008**, 3 (9),
483 563-568 DOI: 10.1038/nnano.2008.215.
- 484 12. Leon, V.; Rodriguez, A. M.; Prieto, P.; Prato, M.; Vazquez, E. Exfoliation of Graphite
485 with Triazine Derivatives under Ball-Milling Conditions: Preparation of Few-Layer Graphene
486 via Selective Noncovalent Interactions. *Acs Nano* **2014**, 8 (1), 563-571 DOI: 10.1021/nn405148t.
- 487 13. Zhou, M.; Tang, J.; Cheng, Q.; Xu, G. J.; Cui, P.; Qin, L. C. Few-layer graphene obtained
488 by electrochemical exfoliation of graphite cathode. *Chem Phys Lett* **2013**, 572, 61-65 DOI:
489 10.1016/j.cplett.2013.04.013.
- 490 14. Milner, E. M.; Skipper, N. T.; Howard, C. A.; Shaffer, M. S. P.; Buckley, D. J.; Rahnejat,
491 K. A.; Cullen, P. L.; Heenan, R. K.; Lindner, P.; Schweins, R. Structure and Morphology of

492 Charged Graphene Platelets in Solution by Small-Angle Neutron Scattering. *J Am Chem Soc*
493 **2012**, 134 (20), 8302-8305 DOI: 10.1021/ja211869u.

494 15. Morishita, T.; Clancy, A. J.; Shaffer, M. S. P. Optimised exfoliation conditions enhance
495 isolation and solubility of grafted graphenes from graphite intercalation compounds. *J Mater*
496 *Chem A* **2014**, 2 (36), 15022-15028 DOI: 10.1039/c4ta02349h.

497 16. Penicaud, A.; Drummond, C. Deconstructing Graphite: Graphenide Solutions. *Accounts*
498 *Chem Res* **2013**, 46 (1), 129-137.

499 17. Valles, C.; Drummond, C.; Saadaoui, H.; Furtado, C. A.; He, M.; Roubeau, O.; Ortolani,
500 L.; Monthieux, M.; Penicaud, A. Solutions of Negatively Charged Graphene Sheets and
501 Ribbons. *J Am Chem Soc* **2008**, 130 (47), 15802-+ DOI: 10.1021/ja808001a.

502 18. Catheline, A.; Valles, C.; Drummond, C.; Ortolani, L.; Morandi, V.; Marcaccio, M.;
503 Iurlo, M.; Paolucci, F.; Penicaud, A. Graphene solutions. *Chem Commun* **2011**, 47 (19), 5470-
504 5472 DOI: 10.1039/c1cc11100k.

505 19. Bepete, G.; Anglaret, E.; Ortolani, L.; Morandi, V.; Huang, K.; Penicaud, A.;
506 Drummond, C. Surfactant-free single-layer graphene in water. *Nat Chem* **2017**, 9 (4), 347-352
507 DOI: 10.1038/Nchem.2669.

508 20. Raji, A. R. O.; Varadhachary, T.; Nan, K. W.; Wang, T.; Lin, J.; Ji, Y. S.; Genorio, B.;
509 Zhu, Y.; Kittrell, C.; Tour, J. M. Composites of Graphene Nanoribbon Stacks and Epoxy for
510 Joule Heating and Deicing of Surfaces. *ACS applied materials & interfaces* **2016**, 8 (5), 3551-
511 3556 DOI: 10.1021/acsami.5b11131.

512 21. Fang, M.; Wang, K. G.; Lu, H. B.; Yang, Y. L.; Nutt, S. Single-layer graphene
513 nanosheets with controlled grafting of polymer chains. *J Mater Chem* **2010**, 20 (10), 1982-1992
514 DOI: 10.1039/b919078c.

515 22. Ye, Y. S.; Chen, Y. N.; Wang, J. S.; Rick, J.; Huang, Y. J.; Chang, F. C.; Hwang, B. J.
516 Versatile Grafting Approaches to Functionalizing Individually Dispersed Graphene Nanosheets
517 Using RAFT Polymerization and Click Chemistry. *Chem Mater* **2012**, 24 (15), 2987-2997 DOI:
518 10.1021/cm301345r.

519 23. Choi, J. H.; Oh, S. B.; Chang, J. H.; Kim, I.; Ha, C. S.; Kim, B. G.; Han, J. H.; Joo, S.
520 W.; Kim, G. H.; Paik, H. J. Graft polymerization of styrene from single-walled carbon nanotube
521 using atom transfer radical polymerization. *Polym Bull* **2005**, 55 (3), 173-179 DOI:
522 10.1007/s00289-005-0426-x.

523 24. Podall, H. F., W.E.; Giraitis, A.P. Catalytic Graphite Inclusion Compounds. I. Potassium
524 Graphite as a Polymerization Catalyst. *The Journal of Organic Chemistry* **1958**, 23 (1), 82-85.

525 25. Shioyama, H. Polymerization of isoprene and styrene in the interlayer spacing of
526 graphite. *Carbon* **1997**, 35 (10-11), 1664-1665 DOI: Doi 10.1016/S0008-6223(97)82797-2.

527 26. Liang, F.; Beach, J. M.; Kobashi, K.; Sadana, A. K.; Vega-Cantu, Y. I.; Tour, J. M.;
528 Billups, W. E. In situ polymerization initiated by single-walled carbon nanotube salts. *Chem*
529 *Mater* **2006**, 18 (20), 4764-4767 DOI: 10.1021/cm0607536.

530 27. Qin, S. H.; Qin, D. Q.; Ford, W. T.; Resasco, D. E.; Herrera, J. E. Functionalization of
531 single-walled carbon nanotubes with polystyrene via grafting to and grafting from methods.
532 *Macromolecules* **2004**, 37 (3), 752-757 DOI: 10.1021/ma035214q.

533 28. Gomez, C. M.; Bucknall, C. B. Blends of Poly(Methyl Methacrylate) with Epoxy-Resin
534 and an Aliphatic Amine Hardener. *Polymer* **1993**, 34 (10), 2111-2117 DOI: Doi 10.1016/0032-
535 3861(93)90737-U.

- 536 29. Sarbu, T.; Lin, K. Y.; Ell, J.; Siegwart, D. J.; Spanswick, J.; Matyjaszewski, K.
537 Polystyrene with designed molecular weight distribution by atom transfer radical coupling.
538 *Macromolecules* **2004**, *37* (9), 3120-3127 DOI: 10.1021/ma035901h.
- 539 30. Leese, H. S.; Govada, L.; Saridakis, E.; Khurshid, S.; Menzel, R.; Morishita, T.; Clancy,
540 A. J.; White, E. R.; Chayen, N. E.; Shaffer, M. S. P. Reductively PEGylated carbon
541 nanomaterials and their use to nucleate 3D protein crystals: a comparison of dimensionality.
542 *Chemical Science* **2016**, DOI: 10.1039/C5SC03595C.
- 543 31. Inagaki, M.; Tanaike, O. Host Effect on the Formation of Sodium-Tetrahydrofuran-
544 Graphite Intercalation Compounds. *Synthetic Met* **1995**, *73* (1), 77-81 DOI: Doi 10.1016/0379-
545 6779(95)03300-9.
- 546 32. Hodge, S. A.; Tay, H. H.; Anthony, D. B.; Menzel, R.; Buckley, D. J.; Cullen, P. L.;
547 Skipper, N. T.; Howard, C. A.; Shaffer, M. S. P. Probing the charging mechanisms of carbon
548 nanomaterial polyelectrolytes. *Faraday Discuss* **2014**, *172*, 311-325 DOI: 10.1039/c4fd00043a.
- 549 33. Schafer, R. A.; Dasler, D.; Mundloch, U.; Hauke, F.; Hirsch, A. Basic Insights into
550 Tunable Graphene Hydrogenation. *J Am Chem Soc* **2016**, *138* (5), 1647-1652 DOI:
551 10.1021/jacs.5b11994.
- 552 34. Ferrari, A. C.; Meyer, J. C.; Scardaci, V.; Casiraghi, C.; Lazzeri, M.; Mauri, F.; Piscanec,
553 S.; Jiang, D.; Novoselov, K. S.; Roth, S.; Geim, A. K. Raman spectrum of graphene and
554 graphene layers. *Phys Rev Lett* **2006**, *97* (18), DOI: Artn 18740110.1103/Physrevlett.97.187401.
- 555 35. Graf, D.; Molitor, F.; Ensslin, K.; Stampfer, C.; Jungen, A.; Hierold, C.; Wirtz, L.
556 Spatially resolved raman spectroscopy of single- and few-layer graphene. *Nano Lett* **2007**, *7* (2),
557 238-242 DOI: 10.1021/nl061702a.
- 558 36. Saikia, B. K.; Boruah, R. K.; Gogoi, P. K. A X-ray diffraction analysis on graphene
559 layers of Assam coal. *J Chem Sci* **2009**, *121* (1), 103-106.
- 560 37. Fujimoto, H. Theoretical X-ray scattering intensity of carbons with turbostratic stacking
561 and AB stacking structures. *Carbon* **2003**, *41* (8), 1585-1592 DOI: 10.1016/S0008-
562 6223(03)00116-7.
- 563 38. Zeng, H. L.; Gao, C.; Yan, D. Y. Poly(epsilon-caprolactone)-functionalized carbon
564 nanotubes and their biodegradation properties. *Adv Funct Mater* **2006**, *16* (6), 812-818 DOI:
565 10.1002/adfm.200500607.
- 566 39. Chadwick, R. C.; Khan, U.; Coleman, J. N.; Adronov, A. Polymer Grafting to Single-
567 Walled Carbon Nanotubes: Effect of Chain Length on Solubility, Graft Density and Mechanical
568 Properties of Macroscopic Structures. *Small* **2013**, *9* (4), 552-560 DOI: 10.1002/sml.201201683.
- 569 40. Degennes, P. G. Conformations of Polymers Attached to an Interface. *Macromolecules*
570 **1980**, *13* (5), 1069-1075 DOI: Doi 10.1021/Ma60077a009.

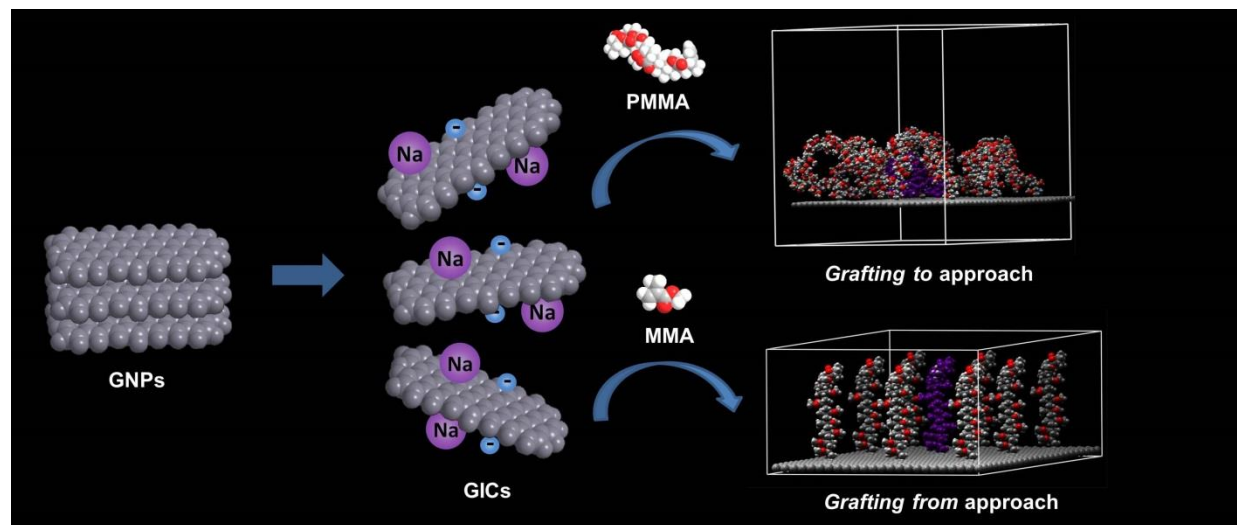
571

572

573

574

575 For table of contents use only



576

577

578